Controlling the onset of traveling pulses in excitable media by nonlocal spatial coupling and time-delayed feedback

Cite as: Chaos **19**, 015110 (2009); https://doi.org/10.1063/1.3096411
Submitted: 18 December 2008 • Accepted: 06 February 2009 • Published Online: 31 March 2009

Felix M. Schneider, Eckehard Schöll and Markus A. Dahlem

Controlling the onset of traveling pulses in excitable media by nonlocal spatial coupling and time-delayed feedback

Felix M. Schneider, Eckehard Schöll, and Markus A. Dahlem
Institut für Theoretische Physik, Technische Universität Berlin, Hardenbergstraße 36, D-10623 Berlin, Germany

(Received 18 December 2008; accepted 6 February 2009; published online 31 March 2009)

The onset of pulse propagation is studied in a reaction-diffusion (RD) model with control by augmented transmission capability that is provided either along nonlocal spatial coupling or by time-delayed feedback. We show that traveling pulses occur primarily as solutions to the RD equations, while augmented transmission changes excitability. For certain ranges of the parameter settings, defined as weak susceptibility and moderate control, respectively, the hybrid model can be mapped to the original RD model. This results in an effective change in RD parameters controlled by augmented transmission. Outside moderate control parameter settings new patterns are obtained, for example, stepwise propagation due to delay-induced oscillations. Augmented transmission constitutes a signaling system complementary to the classical RD mechanism of pattern formation. Our hybrid model combines the two major signaling systems in the brain, namely, volume transmission and synaptic transmission. Our results provide insights into the spread and control of pathological pulses in the brain. © *2009 American Institute of Physics*. [DOI: 10.1063/1.3096411]

Traveling pulses are of fundamental importance in neuroscience. They not only propagate information along the nerve fiber, but are also related to pathological phenomena. Examples are cell depolarizations that lead to a temporary complete loss of normal cell functions in migraine and stroke. This state spreads in cortical tissue via chemical signals that diffuse through the extracellular space. We study these *spreading depolarization* pulses in a standard reaction-diffusion model and suggest to augment the transmission capabilities such that they reflect the cortical structural and functional connectivity. With this new modality, we investigate control of emerging spread of pathological states in the brain.

I. INTRODUCTION

Within the past years control of complex dynamics has evolved as one of the central issues in applied nonlinear science.[1] Major progress has been made in neuroscience, among other areas, by extending methods of chaos control, in particular time-delayed feedback,[2] to spatiotemporal patterns[3–5] and by developing applications in the field of biomedical engineering.[6,7] In this study, control is introduced to suppress spatiotemporal pattern formation. Our emphasis is on understanding the recruitment of cortical tissue into dysfunctional states by traveling pulses of pathological activity, in particular, on internal cortical circuits that provide augmented transmission capabilities and that can prevent such events. Our long-term aim is to design strategies that either support the internal cortical control or mimic its behavior by external control loops and translate these methods into applications.

There is growing experimental evidence that particular spatiotemporal pulse patterns in the human cortex, called *cortical spreading depression*, cause transient neurological symptoms during migraine.[8,9] Similar pulses occur after stroke, called *periinfarct depolarization*, and contribute to the loss of potentially salvageable tissue, i.e., tissue at risk of infarction.[10] These dysfunctional states of the cortex are also referred to as *spreading depolarizations* (SDs) to point out the nearly complete depolarizations of cortical cells and its spread as the common aspect in these patterns.

SD is usually called a cortical *wave*, not pulse, which might cause some confusion. In many cases these two terms can be used interchangeably. We adhere to a precise mathematical terminology, referring to a traveling pulse as a localized event with a spatial profile having a single front and back, while a wave usually refers to a periodic spatial profile. SD is, in this terminology, a pulse. The strict use of this terminology, i.e., to discriminate between pulse and wave, is necessary because of the later (in Sec. II) provided definition of *weak susceptibility*.[11] This definition depends on a bifurcation for which one must strictly distinguish between solitary and periodic wave forms.

The pulse of SD extends in the cortex over several centimeters with a remarkably slow speed of several mm/min. Accordingly, the mathematical description of SD considers large-scale neuronal activity in populations of neurons rather than ion channels in the membrane of nerve fibers, and the spatial coupling is provided by volume transmission, which is essentially a diffusion process. The first mathematical model of SD was proposed by Hodgkin and Grafstein[12] based on bistable rate equations of extracellular K^+ and K^+ diffusion. This model, however, describes only the front dynamics of SD. We suggest (Sec. III) two extensions to this model to study the onset of SD. The first is a necessary extension to obtain onset behavior in the Hodgkin–Grafstein model. We include in a generic form a recovery process for the pulse trailing edge. In the second step, we extend this

model further by nonlocal and time-delayed signal transmission to study the effect of internal control provided as a feedback to the traveling pulse. Results and conclusions are given in Secs. IV and V, respectively.

II. CLASSIFICATIONS OF EXCITABILITY IN LOCAL ELEMENTS AND EXTENDED MEDIA

Excitability, as a property of a single element, is based on threshold behavior and therefore requires a nonlinear process with a stable fixed point. If the system is sufficiently perturbed from this fixed point, it returns after a large excursion in phase space, emitting a spike.[13] If excitable elements are locally interconnected, a new behavior can emerge, namely, the capacity to propagate a sustained pulse through this spatially extended system. This emergent property defines a medium as being excitable, also termed an *active medium*. Excitable elements and excitable media differ in their response to superthreshold stimulation. The response of an excitable element to a superthreshold stimulation will eventually end in the stable fixed point value of the steady state of this element. In contrast, the response of an excitable medium, which is initially in the homogeneous steady state, to a superthreshold stimulation results in approaching a new attractor, the pulse solution. Note, however, that the superthreshold stimulation to evolve in a single pulse must be confined in space and time. For other stimulations, the media would also admit several pulses as solutions or periodic pulse trains, i.e., a traveling wave. However, the different behaviors of local elements and spatial media indicate that there are also different ways to classify excitability in elements and media.

In Sec. II A definitions are provided for excitability of local elements with a focus on neural systems. Some of our results concerning control of spatial-temporal patterns can be explained by considering the effect of control on the local dynamics (Sec. IV B 1). Furthermore, we will consider local dynamics with the aim to extend the Hodgkin–Grafstein model (Sec. III). However, our main focus is on spatial excitability (Sec. II B) and its control by nonlocal and time-delayed feedback described in Secs. IV A and IV B, respectively. For a thorough treatment of local dynamics, in particular in neural systems, see, for example, Ref. 14 or for more complex discharge patterns, such as bursting, see Ref. 15.

A. Local excitability

A generic mechanism of local excitability requires a certain configuration of trajectories in the phase space of a single excitable element (inset in Fig. 1). This configuration usually results from the parameter vicinity of an oscillatory regime whose large amplitude limit cycle is suddenly destructed.[15]

The parameter space is schematically depicted in Fig. 1, where the white area corresponds to the oscillatory regime, and the colored areas mark various regimes of excitability and nonexcitability. If parameter settings are in the excitable regime (to the right of the thick blue dashed line), a rest state (fixed point) is the only attractor. There exists also a threshold close to this rest state, e.g., a "sharp" separatrix or trajectory in phase space (thin dashed line, in the inset). Trajectories starting on the near side of the threshold (green dotted) approach the rest state directly (subthreshold response), while those starting on the far side (red solid) perform a large excursion in phase space, guided by the ghost of a destructed large amplitude limit cycle before returning to the rest state (superthreshold response). Note that we refer to excitable *elements* and not to neurons because also a population of neurons described in a firing rate model can behave like an excitable element.

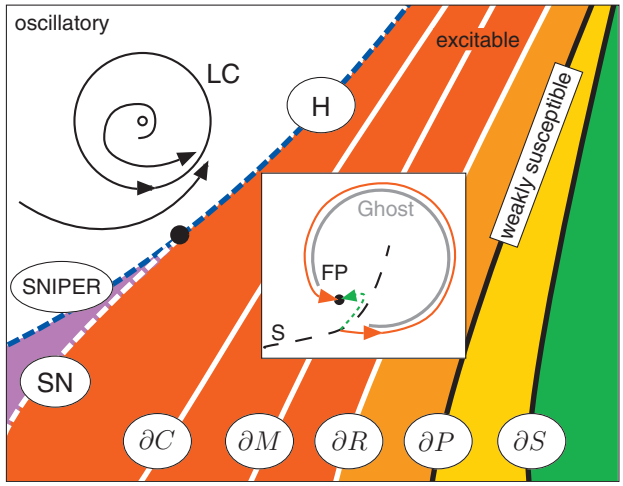

FIG. 1. (Color) Parameter space of excitable systems illustrating a universal scheme for classifications of both local and spatial excitability in general models of active media. Bifurcation lines for excitable elements of an active media are marked by thick blue (dashed) lines. Transitions from the excitable (magenta, red, orange) to the oscillatory regime (white) occur usually either through a SNIPER bifurcation causing excitability of type I, or via a Hopf bifurcation (h) causing excitability of type II. Between the SNIPER and a further SN bifurcation line (magenta) three fixed points (stable node, unstable focus, and saddle) exist in the local excitable elements. The thick white solid lines ∂C, ∂M, and ∂R mark bifurcations of active media where the spatiotemporal pattern in 2D changes (complex, meandering, and rigid rotating spiral patterns, to the left of ∂C, ∂M, and ∂R, respectively). At ∂P the medium becomes nonexcitable. Sustained pulses do not exist in the yellow regime but there is a transient propagating pulse. To the right of ∂S (green) the transient activation radius becomes zero. The insets (thin lines) indicate the corresponding configuration of trajectories in phase space, with limit cycle (LC), sharp separatrix (s), and fixed point (FP).

The way in which, by changing a bifurcation parameter, the dynamics of the local element changes from excitable to oscillatory behavior, that is, the way the large amplitude limit cycle is built up, is used to classify the type of excitability in a single excitable element. This can happen in different ways, two of which are usually distinguished.[14] Type I excitability obtains its characteristic features from a saddle-node infinite period (SNIPER) bifurcation: the frequency of the emerging periodic orbit tends to zero, while the amplitude starts with a finite value. Type II excitability is caused by a Hopf bifurcation, which is characterized by the features that the periodic orbit emerges with zero amplitude and nonzero frequency. In practice, the main characteristic for type II excitability is, however, the onset frequency because for this type a canard explosion renders the zero amplitude practically invisible.

B. Onset of pulse propagation in spatial excitability

The important criterion for spatial excitability is the existence of a traveling pulse solution. In contrast to an excitable local element and its corresponding phase space configuration (inset in Fig. 1), excitability in active media is based on bistability. A superthreshold stimulation takes the system from the homogeneous steady state into the basin of attraction of the pulse solution. The classification of spatial excitability in active media is based on this configuration in phase space. For example, the primary rough classification into excitable and nonexcitable media is based on the existence and nonexistence, respectively, of the pulse as the most basic spatiotemporal pattern that sustainedly propagates in space. This *propagation boundary* is called ∂P.[16] The focus in this study is on the onset of excitability in active media at ∂P.

The propagation boundary ∂P is determined in the parameter space of a comoving frame. In this frame, ∂P is caused by a saddle-node bifurcation above which traveling pulse solutions exist. As active media are usually based on a reaction-diffusion (RD) mechanism, this bifurcation is computed in a parabolic partial differential equation (PDE). The details of this computation can be found in textbooks[17] and have been further related to the phenomenon of SD in the cortex in Ref. 3. Therefore, we just sketch the basic idea. The propagation boundary in a parabolic PDE is obtained by searching pulse profiles as stationary solutions in a comoving frame. The pulse solution of the profile equation in the comoving frame must tend to the fixed point value of the original system for $\xi \rightarrow \pm\infty$, with ξ being the spatial coordinate in the comoving frame. A traveling pulse is thus equivalent to the existence of a homoclinic orbit satisfying a system of ordinary differential equations, namely, the profile equation system, with appropriate boundary conditions. ∂P is determined numerically by continuation of a homoclinic orbit in this profile equation detecting the saddle-node bifurcation, where two homoclinic orbits corresponding to a fast and a slow pulse solution collide and annihilate. For higher values of ε, β, or γ no stationary pulse solution exists.

In Sec. IV we describe how the locus of the propagation boundary ∂P in the parameter space is controlled by nonlocal spatial coupling and time-delayed feedback by a shift to new parameter values without adding a distinctly new character to the spatiotemporal patterns, as schematically illustrated in Fig. 2. Since the propagation boundary is essentially a feature of an active medium with one spatial dimension, we can limit our main investigation to one-dimensional (1D) systems. Yet, to get a picture of the patterns that arise in the neighborhood of ∂P, we will end Sec. II by a brief review of patterns in higher spatial dimensions and provide definitions of *weak excitability* and *weak susceptibility*.

C. Weak excitability and weak susceptibility

The variety of qualitatively different spatiotemporal patterns in higher excitable regimes, i.e., beyond ∂P toward the oscillatory regime (to the left of ∂P in Fig. 1), provides the foundation for a classification of spatial excitability in active media. This is in so far analogous to the classification into types I and II of excitable local elements (Sec. II A) as both classifications are built on the patterns that emerge. However, the classification of local excitability defines different types of mechanisms, whereas the classification of spatial excitability characterizes rather the degree of excitability.

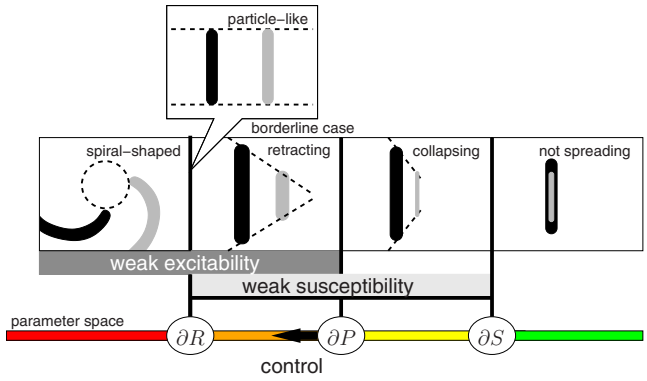

FIG. 2. (Color online) Scheme of the classification of excitability according to spatiotemporal patterns (spiral-wave, particlelike, retracting, collapsing, and no spread) in 2D: wave front at two instances in time (t_1: black, t_2: gray) and trajectory of open wave ends (dashed). This scheme illustrates the effect of control on the propagation boundary (∂P) by additional nonlocal and time-delayed transmission capabilities. ∂P is controlled by shifting the bifurcation in parameter space [horizontal (multicolored) line]. This affects the regime of weak susceptibility centered around ∂P and bounded by the rotor boundary ∂R and the spreading boundary ∂S.

Excitability is described by ordinary differential equations in local elements and by PDEs in spatial media. Roughly speaking, the additional independent spatial variable allows for more complex patterns due to the fact that the spatial dimension renders the phase space infinite dimensional. In fact, the patterns can become even more complex if spatial dimensions are increased from one to two (for example, spiral waves in retinal spreading depression[18]) or three dimensions (Winfree turbulence of scroll waves in cardiac fibrillation[19]).

Close to the propagation boundary, the complexity of emerging patterns is largely independent of the number of spatial dimensions. This fact is also paraphrased as *weak excitability*.[20] This term is used for active media to indicate that either no reentrant patterns occur (described by the rotor boundary ∂R,[16] see Figs. 1 and 2) or that the rotation period is large enough, so that the front of the pulse does not interact with its refractory back. The onset of interactions between front and refractory back in a re-entrant wave pattern is described by the meandering boundary ∂M (see Fig. 1). To the left of this boundary, the core of a freely rotating spiral wave performs a meandering pattern,[21,22] whereas to the right of ∂M, the spiral core follows a rigidly circular rotation[23] (Fig. 2). Changing excitability parameters further, the spiral core can start to perform more complex maneuvers to avoid the refractory zone (complex boundary ∂C) (see Fig. 1).

Patterns of spreading depression in chicken retina are observed *in vitro* in the complex regime to the left of ∂C,[18] but in human brain tissue they occur close to ∂R. It was predicted that the window of cortical excitability lies between ∂R and ∂P (Ref. 24) and this seems to be confirmed by a functional magnetic resonance imaging study in migraine,

mapping spatiotemporal patterns of symptom reports onto the folded cortical surface.[25] These patterns are similar to particlelike or retracting wave segments that occur between ∂R and ∂P.[26–28] Transient patterns can also be observed at even lower excitability, limited by the spreading boundary ∂S (Ref. 29) (Fig. 2). Since the regime of retracting wave segments is not identical to weak excitability (absence of front-back interactions), it was called weak susceptibility based on a susceptibility scale that can also be operationally defined in experimental systems.[25] The control of excitability in media being weakly susceptible to pattern formation can be investigated in a model with one spatial dimension because ∂P is essentially a property of a 1D parabolic PDE.

III. REACTION-DIFFUSION WITH AUGMENTED TRANSMISSION CAPABILITY

The generic framework to model spatial excitability is a RD system of activator-inhibitor type. In fact, already a single species model has the capacity to propagate fronts.[30] Such a model was originally suggested for SD by Hodgkin and Grafstein[12] (Sec. III A). We extend this generic model by choosing appropriate inhibitor dynamics (Sec. III B) to obtain pulses with the onset saddle-node bifurcation ∂P and introduce augmented transmission capabilities (Sec. III C).

A. Hodgkin–Grafstein model

A single species model of bistability has the capacity to propagate one state into the other if these bistable dynamics of the species, called u, are coupled by diffusion

$$\frac{\partial u}{\partial t} = f(u) - v + \frac{\partial^2 u}{\partial x^2}, \tag{1}$$

$$f(u) = u - \frac{u^3}{3}. \tag{2}$$

Here v is a bifurcation parameter. In these nondimensional equations, the diffusion coefficient, which merely scales space, is set to unity.

Equations (1) and (2) were proposed by Hodgkin as a model for spreading depression based on the bistable K^+ dynamics suggested by Grafstein.[12] The front profile of the species u and its speed can be calculated analytically for the cubic polynomial form of $f(u)$, i.e., the generic form of bistable dynamics (see, for example, the textbook in Refs. 31 and 32). In the context of control one should think of the two stable states as one being a physiological (healthy) state and the other one being a pathological (depolarized) state, and the latter invading the former, which shall be prevented by control.

As is shown in Sec. IV, control of the onset of propagation depends essentially on the interaction of the healthy state with the pulse front via the augmented transmission capability. However, in the system defined by Eqs. (1) and (2) there does not exist a boundary like ∂P (Sec. II B). In other words, there is no abrupt onset of the capacity to propagate fronts with finite speed. Instead, the heteroclinic orbit, which corresponds to the front profile in a comoving frame, exists for the whole bistable regime, in particular also for arbitrarily slow velocities of the comoving frame including zero (standing front).[31] To obtain propagation onset behavior, we need to add inhibitor dynamics, i.e., a second recovery species for the Hodgkin–Grafstein model.

B. Extension by inhibitor dynamics

With a proper choice of a second species whose dynamics is coupled to u, the local system can change from bistable to excitable dynamics, which is needed to observe and compute ∂P. The natural choice is to use the bifurcation parameter v of the Hodgkin–Grafstein scheme as the additional species, namely, as an *inhibitor*,

$$\frac{\partial v}{\partial t} = \varepsilon g(u,v). \tag{3}$$

The rate function $g(u,v)$ of the inhibitor determines the dynamics in the refractory phase of the pulse, where it recovers the initial healthy state that was recruited into the pathological state of species u. In this two-species model, u is called the *activator*. Inhibitor dynamics usually changes on a slower time scale $\varepsilon \ll 1$.

There are several models in the neuroscience literature obeying this structure in Eqs. (1)–(3), both models with local excitability of type I (Refs. 31 and 33) and of type II.[34–36] These models are, however, models of action potentials describing the propagation of normal electrophysiological activity along single nerve fibers. Therefore these models do not relate directly to SD because SD is caused by large-scale neuronal activity.[37,38] Therefore the analogy to models as in Refs. 31 and 33–36 is mainly formal in the mathematical structure but not in its biological interpretation. For example, in the Hodgkin–Grafstein equation [Eqs. (1) and (2)], the activator is K^+, while in action potential models it is the membrane potential.

Models exhibiting type I excitability are also capable to show type II behavior for a certain parameter regime but the reverse is not necessarily true. This suggests that type II behavior is more generic because it can be observed in both types of models and only requires a rate function $g(u,v)$ that is linear in both arguments. We introduce inhibitor dynamics as

$$g(u,v) = u + \beta - \gamma v. \tag{4}$$

With this choice, the local excitable dynamics is of type II. The parameters β and γ determine the precise configuration of trajectories in phase space that lead to excitability and are thus, in addition to ε, the only two parameters that control excitability of type II in a normal form model.

Equations (1)–(4) correspond to the well studied FitzHugh–Nagumo (FHN) systems, which is, in fact, used as a paradigm for excitable systems.[13] Pattern formation in a net of FHN elements under the influence of time-delayed feedback was investigated with the aim to increase the coherence of noise-induced wave patterns.[39,40] In the excitable regime the system has one fixed point, depending on the parameters β and γ. For the setting (β=0.85, γ=0.5), the fixed point is (u^*=−1.1684, v^*=−0.6367).

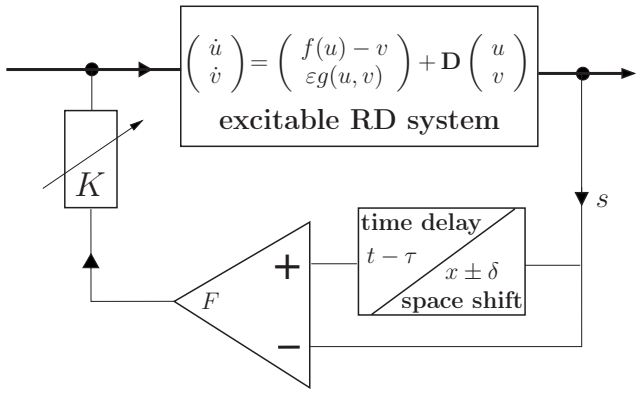

FIG. 3. Diagrammatic view of control by augmented transmission (CAT).

C. Augmented transmission capability

We extend the FHN model by introducing augmented transmission capability into Eqs. (1)–(4) as a feedback loop[41]

$$\begin{pmatrix} \partial_t u \\ \varepsilon^{-1}\partial_t v \end{pmatrix} = \begin{pmatrix} f(u)-v \\ g(u,v) \end{pmatrix} + \mathbf{D}\begin{pmatrix} u \\ v \end{pmatrix} + \mathbf{H}\begin{pmatrix} u \\ v \end{pmatrix}, \tag{5}$$

where **D** is the local diffusion operator, and **H** represents the augmented transmission capability. In Eqs. (1)–(4) we have considered diffusion in the activator species u only:

$$\mathbf{D} = \begin{pmatrix} \nabla^2 & 0 \\ 0 & 0 \end{pmatrix}. \tag{6}$$

The augmented transmission capability

$$\mathbf{H} = K\mathbf{F} \tag{7}$$

is described by the control strength K and the control matrix

$$\mathbf{F} = \begin{pmatrix} F_{11} & F_{12} \\ F_{21} & F_{22} \end{pmatrix}, \tag{8}$$

whose element F_{ij} are operators which represent three individual steps of the control by augmented transmission (CAT), namely, (i) selecting a species j whose transmission capability is augmented, (ii) creating the control force from this species, and (iii) feeding this control force back into the dynamical variable i (see Fig. 3).

Formally, this can be represented by splitting $F_{ij}=A_{ij}F$ into the components of a coupling matrix **A**, which represents the coupling scheme, and an operator F that creates the type of control signal. For instance, **A** may be chosen as one of the following:

$$\mathbf{A}^{uu} = \begin{pmatrix} 1 & 0 \\ 0 & 0 \end{pmatrix}, \quad \mathbf{A}^{uv} = \begin{pmatrix} 0 & 1 \\ 0 & 0 \end{pmatrix},$$
$$\mathbf{A}^{vu} = \begin{pmatrix} 0 & 0 \\ 1 & 0 \end{pmatrix}, \quad \mathbf{A}^{vv} = \begin{pmatrix} 0 & 0 \\ 0 & 1 \end{pmatrix}, \tag{9}$$

where the upper indices label the coupling scheme, e.g., $\mathbf{A}^{uu}$ denotes a matrix representing the coupling scheme uu.

The control signal F is generated from the input variable $s=u$ or $s=v$ by time-delayed or nonlocal feedback. For example, in time-delayed feedback as introduced by Pyragas,[2] the operator F creates the difference between the time-delayed signal $s(t-\tau)$ and its current counterpart $s(t)$. We study this type and two nonlocal types of coupling. The control force F of these different types, as a function of the signal s, is described in detail in Secs. IV A and IV B. It should be noted that in Eq. (5), **H** represents cortical circuits[42] and neurovascular coupling,[3] that is, *internal* control loops.

The four coupling matrices in Eq. (9) lead to four transmission pathways, also termed *coupling schemes*: two self-couplings uu and vv, and two cross-coupling vu and uv, corresponding to the upper indices ij in Eq. (9). Note that other coupling schemes represented by the coupling matrix **A**, for example, diagonal coupling or coupling with a rotation matrix,[5,43,44] can also be investigated within this framework.

IV. SUPPRESSION OF PULSE PROPAGATION

We perform simulations of the RD system in Eqs. (1)–(4) in one spatial dimension with RD parameter settings ($\varepsilon=0.1$, $\beta=0.85$, and $\gamma=0.5$) for the weakly excitable regime close to the propagation boundary ∂P (Sec. II B). The RD system is extended by three types of coupling in the framework of Eq. (5), i.e., two types of nonlocal spatial coupling (isotropic and anisotropic) and one type of time-delayed feedback. In the context of SD, nonlocal spatial and local time-delayed couplings represent neural structural and functional connectivity and neurovascular feedback in the cortex. This is discussed in more detail in Ref. 3. For each type of coupling there are four principal coupling schemes, two self-coupling schemes (uu,vv) and two cross-coupling schemes (uv,vu), defined by the coupling matrix **A** in Eq. (9).

We initialize each simulation with a stable pulse profile solution of the RD system in Eqs. (1)–(4) to investigate the effect of control on RD excitability. This is accomplished by testing whether this specific initial condition of the free system (RD only) is in the basin of attraction of the homogeneous steady state of Eq. (5), i.e., the controlled system (RD-CAT). There are two CAT parameters: the control gain K in Eq. (7), and a spatial (δ) or temporal (τ) control scale, respectively, which will be introduced in Secs. IV A and IV B. For a large range of these two CAT parameters, we determine whether pulse propagation is suppressed or not. The propagation is suppressed if the excitation dies out, so that the system approaches the homogeneous steady state. In this case, CAT is considered successful. In the reverse case, any sustained spatiotemporal pattern that evolves from the initial conditions (free pulse solution), after the CAT is "switched on," is considered an unsuccessful control since the activity is not completely suppressed and the homogeneous steady state is not reached.

For the following simulations we adopt an active medium with a spatial extension of $L=160$. As spatial increment in the discretized Laplacian **D** we take $\delta x=0.2$. All simulations are run for 2000 time units and use an Euler forward algorithm with discretization $\delta t=0.001\,25$. The spatial and temporal widths of the free-running activator pulse, Δx and Δt, respectively, serve as reference space and time scales.[3] In the dimensionless units of the FHN system, the pulse width

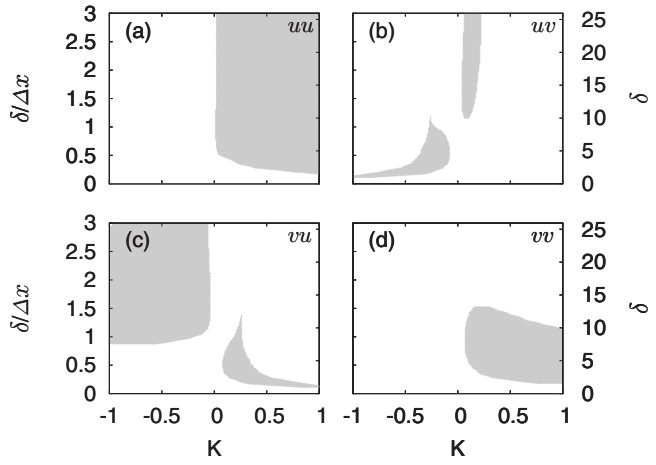

FIG. 4. Control planes of isotropic spatial coupling spanned by the two CAT parameters: control gain factor K and nonlocal space scale δ normalized to pulse width Δx (left scale) and in spatial units (right scale). (a) Activator self-coupling scheme uu, (b) cross-coupling uv (inhibitor signal fed back to activator rate equation), (c) vu (reverse), and (d) inhibitor self-coupling vv. Suppression of pulse propagation is marked by gray control domains. Parameters: $\varepsilon=0.1$, $\beta=0.85$, $\gamma=0.5$, and $\Delta x=8.65$.

measured at the level of 5% of the excess value above the homogeneous fixed point level is $\Delta x=8.645$ or $\Delta t=10.7274$.

A. Pulse suppression by nonlocal spatial coupling

In this section we present results on two types of spatial coupling.

1. Isotropic coupling

Nonlocal isotropic spatial coupling is defined as

$$F(s)=s(x+\delta,t)+s(x-\delta,t)-2s(x,t), \tag{10}$$

where $s=u$ or $s=v$.

Regimes in which RD pulses are suppressed by additional nonlocal connections are calculated for the parameters δ and K and represented by gray areas in Fig. 4. For the two self-coupling schemes uu and vv, shown in Figs. 4(a) and 4(d), respectively, the sign of the gain parameter K determines the effect of the nonlocal connection. Pulse propagation can only be suppressed for $K>0$. For the two cross-coupling schemes uv and vu, shown in Figs. 4(b) and 4(c), respectively, the sign of the gain parameter K changes at $\delta\approx\Delta x$ for pulse suppression, and these two cross-coupling schemes show similar control domains with respect to reflection $K\to -K$.

The sign of K in the control domains of the self-coupling schemes [Figs. 4(a) and 4(d)] can be qualitatively understood by considering the effect of nonlocal connections upon the homogeneous steady state in the limit $\delta\to 0$. For $K>0$, this limit corresponds to diffusively coupled elements. In general, the homogeneous steady state is stabilized by diffusion against small inhomogeneous perturbations. In the same way, a local perturbation is leveled by a nonlocal connection in the form of Eq. (10) for self-coupling. In the diffusion limit, however, K would increase the diffusion coefficient, which causes the pulses to become broader. Yet, a qualitative change in the dynamics cannot occur by changing the diffusion coefficient. Therefore the effect of suppressing pulses depends on the nonlocal character of the connection, which must extend at least over a distance of about 20% of the pulse width Δx, as can be seen by the onset of the control domain at values of $\delta/\Delta x>0.2$ in Figs. 4(a) and 4(d).

The control domains of the cross-coupling schemes [Figs. 4(b) and 4(c)] are qualitatively different from self-coupling. K changes its sign at $\delta\approx\Delta x$ within one scheme and, accordingly, the situation of pulse suppression is more complex. There is a long-range regime ($\delta>\Delta x$) and a short-range regime ($\delta<\Delta x$).

2. Anisotropic backward coupling

Nonlocal connections can also be introduced in only one direction

$$F(s)=s(x\pm\delta,t)-s(x,t). \tag{11}$$

This directed connectivity would correspond to anisotropic nonlocal coupling in a two-dimensional (2D) excitable medium. One reason to investigate this type of connectivity is to obtain a better understanding of the results in the Sec. IV A 1 by separating effects of forward and backward connections [Fig. 5(a)]. Moreover, the functional and structural connectivity of the cortex is realistically modeled as an anisotropic (and also inhomogeneous) medium due to the patchy nature of nonlocal horizontal cortical connections. While anisotropies in the cortical connections are usually considered to merely cause variations in wave speed in different directions, inhomogeneities are known to cause wave propagation failure.[45] In contrast, our focus is on the change in excitability by anisotropic nonlocal coupling that leads to suppression of wave propagation.

We limit your investigation to the backward connection. This corresponds to the plus (minus) sign in Eq. (11) for pulses propagating in the positive (negative) x direction

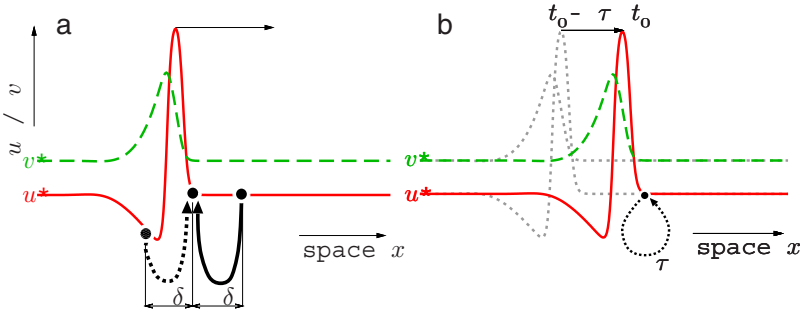

FIG. 5. (Color online) Schematic diagram illustrating nonlocal spatial coupling and time-delayed feedback. (a) Nonlocal spatial coupling: isotropic coupling (dashed and solid arrow) and anisotropic backward coupling (solid arrow). (b) Time-delayed feedback: backward coupling of traveling pulses. Pulse profiles are shown in red (solid) and green (dashed) for the activator and inhibitor, respectively. Dotted: time-delayed profiles.

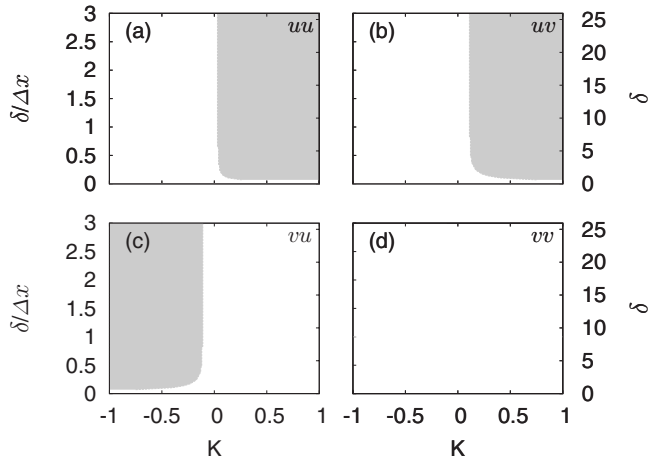

FIG. 6. Control planes of anisotropic backward spatial coupling. Parameters and notation as in Fig. 4.

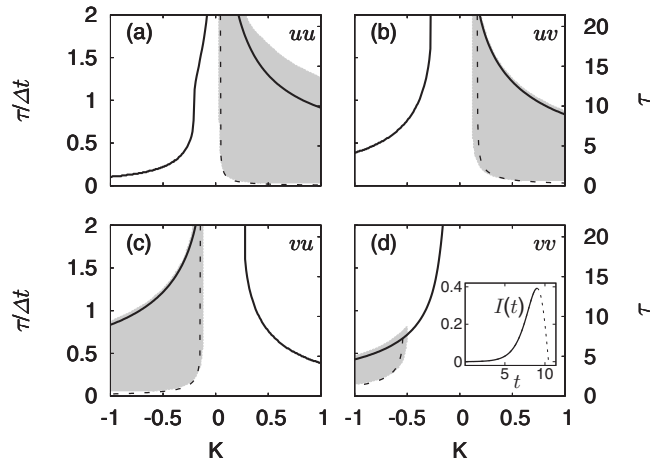

FIG. 7. Control planes of time-delayed feedback coupling spanned by the two CAT parameters: control gain factor K and time delay τ normalized to pulse width Δt (left scale) and in temporal units (right scale). (a) Activator self-coupling scheme uu, (b) cross-coupling uv (inhibitor signal fed back to activator rate equation) and (c) vu (reverse), and (d) inhibitor self-coupling vv. Suppression of pulse propagation is marked by gray control domains. The black lines denote saddle-node bifurcations, which were also found and investigated in detail in two delay-coupled FHN systems (Refs. 46 and 47). The dashed lines mark the values of control parameters for which the u-amplitude of a single local FHN system, stimulated in u by $I(t)$ [shown as inset in (d)], is decreased by 10% compared to the u-amplitude of the uncontrolled system. Parameters as in Fig. 4, $\Delta t=10.73$.

[solid arrow in Fig. 5(a)]. We choose the backward connection because this type of coupling shares many properties with local time-delayed feedback coupling, as we will show by comparing the results from this section with those of Sec. IV B.

The control domain of the uu self-coupling scheme [Fig. 6(a)] is very similar to the isotropic one shown in Fig. 4(a). This indicates that in the uu scheme of isotropic coupling the backward connection accounts for the main contribution to suppression of wave propagation. However, we want to note that both control types (isotropic and anisotropic) with the same coupling scheme uu can differ in their efficiency within some parts of the gray control domain (not shown). The efficiency refers to the length a pulse travels after the connectivity is switched on. This transient effect was investigated in detail in Refs. 3 and 29, whereas in this study we concentrate on an understanding of the size and shape of control domains for the different schemes and types of coupling (Figs. 4, 6, and 7).

Pulse propagation is not suppressed by the vv self-coupling scheme for anisotropic backward coupling for any control parameter within the investigated range [Fig. 6(d)]. This, however, does not mean that the pulse propagates essentially unchanged. Any sustained spatiotemporal pattern other than the homogeneous steady state that evolves from the free initial pulse solution—after the connectivity is switched on—is considered as unsuccessful pulse suppression. In fact, for the vv scheme of anisotropic coupling in the expected control domain of corresponding Fig. 4(d), the homogeneous steady state becomes unstable and stationary spatial patterns emerge after the initial pulse is suppressed.

The control domains of the cross-coupling schemes [Figs. 6(b) and 6(c)] are similar to Figs. 4(b) and 4(c) in the long-range regime except for a failure of suppression in the isotropic uv scheme for $K>0.2$. The long-range regime for anisotropic backward cross coupling extends over the nearly complete spatial scale of δ (except for very small δ). Thus, K does not change its sign. Also, there is a perfect reflection symmetric pattern in the control planes with respect to the axis $K=0$ for the two cross-coupling schemes. This led us to conclude that the sign of K for pulse suppression in the long-range regime of isotropic coupling depends mainly on the backward connection [solid arrow in Fig. 5(a)]. In the short-range regime, the effect of the forward connection [dotted arrow in Fig. 5(a)] seems to dominate and oppose the effect of the backward connection.

The reason for the reflection symmetry in the pattern of control domains for cross-coupling schemes and, furthermore, the explanation for the observed signs of the gain parameter K for the control domains of all coupling schemes for anisotropic backward coupling are given in Sec. IV C together with the explanation of some of the results we have obtained for local time-delayed feedback control (Pyragas feedback), which will be described in Sec. IV B.

B. Pulse suppression by local time-delayed feedback

In case of local time-delayed feedback, the control force F is given by

$$F(s) = s(x,t-\tau) - s(x,t), \tag{12}$$

where τ is the delay time. Note the formal similarity to Eq. (11). This control method was first introduced by Pyragas[2] for chaos control. In Fig. 5(b), this control method is illustrated for the uu coupling scheme: at each spatial location x the activator u at time t receives the signal from the same location but at the past time $t-\tau$. That means particularly for the dynamics of the front that the deviation from the homogeneous fixed point is fed back.

The domains of successful control, i.e., pulse suppression, in the (K,τ) plane are shown as gray areas in Fig. 7. For successful control, the pulse dies out and the system returns to the homogeneous steady state, as shown exemplarily in the space-time plot of Fig. 8(b).

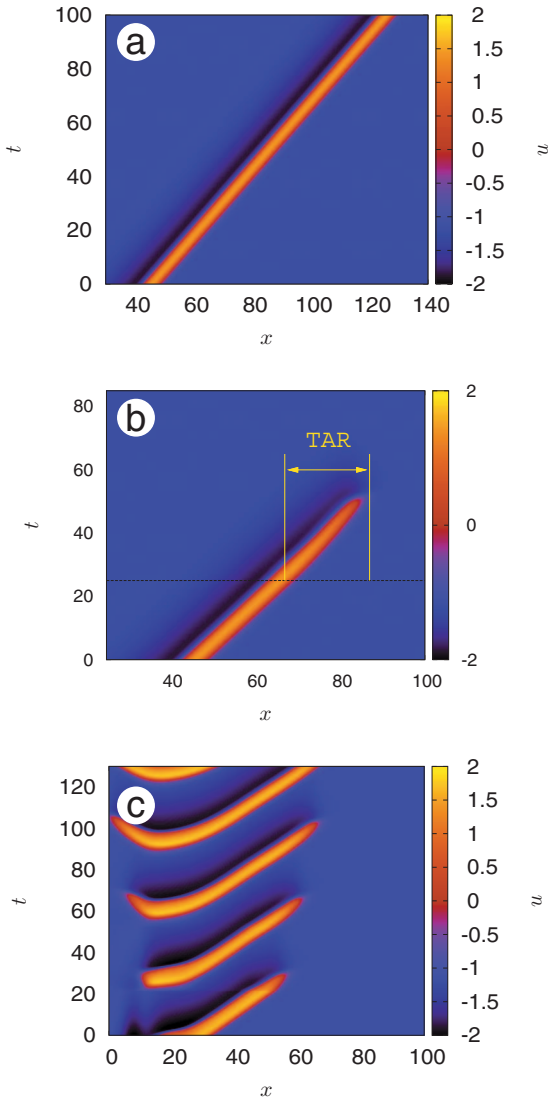

FIG. 8. (Color) Pattern formation for $\varepsilon=0.1$, $\beta=0.85$, and $\gamma=0.5$: (a) pulse propagation without control; (b) suppressed pulse via nonlocal coupling ($K=0.2$ and $\delta=0.58\Delta x$). The horizontal line at $t=25$ marks the onset of control. After the control is activated the excitation becomes transient. The distance that the transient excitation spreads before it relaxes to the homogeneous fixed point defines the transient activation radius (TAR) also referred to as *tissue at risk* (cf. Ref. 3). (c) Delay-induced oscillatory tracking pattern ($K=0.5$, $\tau=2.8\Delta t$, onset of control at $t=21$).

For time-delayed feedback, a domain of successful control exists for each coupling scheme. As for the spatial coupling schemes in Figs. 4 and 6, the two cross-coupling schemes uv and vu show a reflection symmetry with respect to the axis $K=0$. This symmetry is explained by the effective parameters introduced in Sec. IV C. Coupling schemes that feed back the signal to the activator can suppress pulses for positive K. For coupling schemes that feed back the signal to the inhibitor, successful control is possible for negative values of K. This is similar to the results of anisotropic backward coupling (cf. Fig. 6). This similarity is due to the similarity of the signals the pulse receives through the feedback. In both cases the wave front gets the feedback from the homogeneous steady state which is ahead of the wave, in a temporal or spatial sense, respectively.

The main differences between the control domains of time-delayed feedback and spatial anisotropic coupling are that in the case of time-delayed feedback the control domains are limited toward large values of τ [upper borders of gray domains in Figs. 7(a)–7(d)], and, moreover, that there is a control domain also for vv, the inhibitor self-coupling scheme. The limitation of the control domains toward large values of τ is caused by the formation of tracking patterns[48] (Fig. 8), which is further explained in Sec. IV B 2. These patterns emerge by delay-induced oscillations. The local dynamics becomes bistable due to a saddle-node bifurcation (black solid lines, Fig. 7). This is demonstrated in Sec. IV B 1 and IV B 2.

1. Effect of time-delayed feedback in a local excitable system

In this section we investigate the effect of time-delayed feedback on a single local excitable element. There are two main effects. First, depending on the sign of the control parameter K and the coupling scheme, the activator amplitude is reduced, which selects the location of the control domain in the control plane with respect to the axis $K=0$ (Fig. 7). Furthermore, we show that a minimum amplitude reduction of about 10% is needed to suppress pulse propagation when these elements form an active medium (lower bounds of the control domains). Second, for too large a value of τ, the local dynamics becomes bistable (upper bounds of the control domains).

To obtain qualitative insight into how time-delayed feedback operates, we perform numerical simulations in order to compare trajectories starting from the same initial conditions with and without time-delayed feedback. Figure 9 shows exemplary superthreshold phase space excursions with and without ($K=0$) time-delayed feedback (solid and dashed trajectories, respectively). The system is initialized in the interval $[t_0-\tau;t_0[$ (history function) with the fixed point value ($u=u^*$ and $v=v^*$) and for t_0 with a superthreshold value ($u=u^*+0.5$ and $v=v^*$).

For coupling schemes that feed back into the activator rate equation, i.e., uu and uv, the control force acts parallel to the u axis. In Fig. 9(a) the trajectories with and without control for the uu coupling scheme are plotted. The direction of the control force is denoted by the horizontal arrow. In order to reduce the amplitude in u, the control force has to be directed toward the fixed point, i.e., it has to be negative for $u>u^*$ and $v>v^*$. This is the case for $t<\tau$ if $K>0$ because the history function is initialized as (u^*,v^*).

For the vu and vv coupling scheme, the control force acts parallel to the v-axis. In Fig. 9(b) the trajectories with and without control are shown for vv coupling. The direction of the control force is denoted by the vertical arrow. To get lower amplitudes of u, the control force has to be directed toward the opposite direction of the fixed point. This is the case for $t<\tau$ if $K<0$.

In the following, the reduction in the amplitude u of a single local FHN system is investigated in order to obtain the lower boundaries (dashed) of the control domains in Fig. 7. To excite the system a stimulation current $I(t)$ [inset of Fig. 7(d)] is added to the activator u. To obtain a stimulation

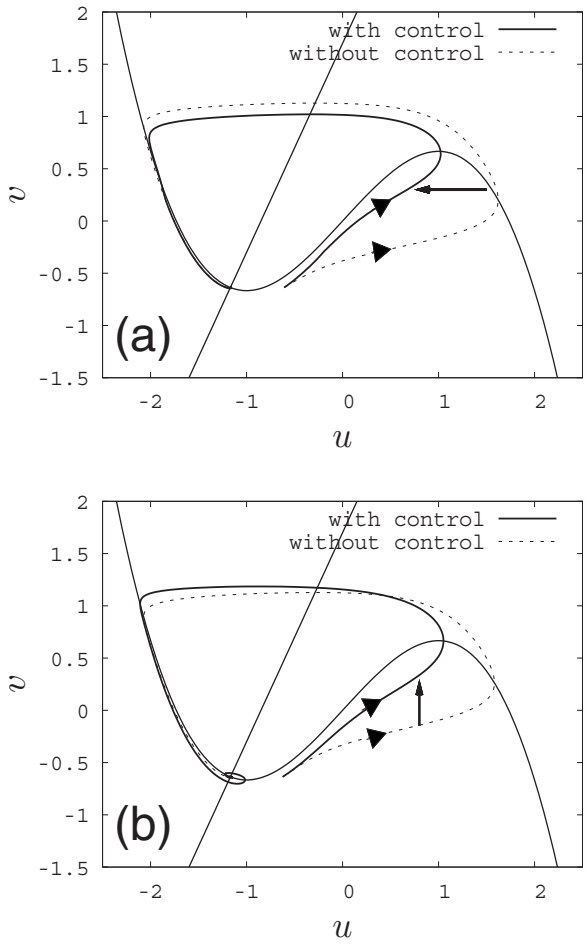

FIG. 9. Phase portraits of a local FHN system with (solid trajectory) and without (dashed trajectory) time-delayed feedback control. (a) uu coupling: $K=0.03$, (b) vv coupling: $K=-0.7$. Parameters: $\varepsilon=0.1$, $\beta=0.85$, $\gamma=0.5$, and $\tau=5$, no diffusion. The solid arrow denotes the action of the control force.

current of suitable magnitude, we record the diffusion signal fed into a local FHN element as a pulse is passing. $I(t)$ is this signal, whereas we only use it as a stimulation current up to its maximum value (solid line). The dotted line denotes the further evolution of this signal.

Choosing for each coupling scheme the proper sign of control gain K to reduce the activator amplitude, time-delayed feedback is activated and the maximum amplitude $u_{\max}$ is observed. By performing a bisection method for each value of K, the proper τ is detected that reduces $u_{\max}$ by 10% from the original amplitude after stimulation without feedback ($K=0$). The dashed lines in Fig. 7 mark the positions where the u-amplitude is reduced by 10% for a fixed stimulation. These lines form the lower boundaries of the control domains.

Also the upper boundaries of the control domains can be understood by investigating the single system with feedback. For large K and τ the system becomes bistable in the sense that in addition to the stable fixed point a stable limit cycle occurs. This limit cycle appears in a saddle-node bifurcation of limit cycles, as was also found in a system of two delay-coupled FHN systems.[46,47] The limit cycle emerges if (i) τ is sufficiently large to allow for recovery to the fixed point, and (ii) the feedback and, hence, the gain parameter K are strong enough to push the system beyond the threshold.

Again with the help of a bisection method, the saddle-node bifurcation lines for the single system are determined in the (K,τ)-plane. In Fig. 7 they are plotted as black solid lines. These lines mark the boundaries where the local dynamics becomes bistable and control fails. Only in the case of uu coupling the boundary of the control domain deviates appreciably from this bifurcation line. This is due to the stabilizing effect of diffusion that damps out local oscillations. Since in the interspace the single system is bistable and thus the medium is able to perform homogeneous oscillations, the difference between the upper boundary of the control domain and the bifurcation line depends on the initial conditions that are chosen to locally stimulate the medium.

Investigating a single FHN element with time-delayed feedback provides a qualitative understanding of the dynamics of the controlled spatial system: the sign of K and the form of the control domains can be understood. Thus the control of local excitability provides control of the global spatial excitability. This will be quantified in Sec. IV C. In Sec. IV B 2, we present the spatiotemporal patterns that emerge above the upper boundary of the control domain, i.e., the bistable domain of the single local element.

2. Delay-induced oscillatory pattern formation

As we have seen in Sec. IV B 1, the local FHN dynamics with time-delayed feedback becomes bistable for too large values of K and τ. Due to this local bistability, in the spatially extended system delay-induced oscillatory pattern formation occurs [Fig. 8(c)]: after a local stimulation, the medium performs local oscillations that spread slowly. Within each local oscillation, the excitation spreads a short way, and thus gradually new parts in the neighborhood become excited. The area of oscillatory excitation grows slowly all over the medium. We have observed these patterns for each coupling scheme beyond the upper boundary of the control domain.

This effect will again play an important role in Sec. IV C 2, that focuses on the propagation boundaries in (ε,β)-parameter space.

C. Description through effective parameters

In this section we further investigate the two control schemes of spatial anisotropic backward coupling and local time-delayed feedback to achieve an analytic approximation. In Sec. IV C 1 we use this to describe the change in excitability and in Sec. IV C 2 we investigate how this is reflected in the parameter space.

For our approximation we assume that the front dynamics governs the location of the propagation boundary ∂P. Therefore we focus on the part of control that acts on the front dynamics. For the coupling types of time-delayed feedback and nonlocal anisotropic coupling, the front of the pulse receives the feedback of the homogeneous steady state. The main idea is to replace the time delayed [in Eq. (12)] or the space-shifted [in Eq. (11)] quantities by their fixed point values $[u(x,t-\tau)=u(x+\delta,t)=u^*$ and $v(x,t-\tau)=v(x+\delta,t)=v^*]$.

TABLE I. Effective parameters and transformations for coupling schemes uu, uv, vu, and vv.

	uu	uv	vu	vv
$\tilde{t}$	$t(1-K)$	t	t	t
$\tilde{x}$	$x\sqrt{1-K}$	x	x	x
$\tilde{u}$	$\frac{u}{\sqrt{1-K}}$	u	u	u
$\tilde{v}$	$\frac{(v-Ku^*)}{\sqrt{1-K^3}}$	$v-K(v^*-v)$	v	v
$\tilde{\varepsilon}$	$\frac{\varepsilon}{(1-K)^2}$	$(1+K)\varepsilon$	$(1-K)\varepsilon$	ε
$\tilde{\beta}$	$\frac{(\beta-\gamma Ku^*)}{\sqrt{1-K}}$	$\frac{\beta-Ku^*}{1+K}$	$\frac{\beta+Ku^*}{1-K}$	$\beta+Kv^*$
$\tilde{\gamma}$	$\gamma(1-K)$	$\frac{\gamma}{1+K}$	$\frac{\gamma}{1-K}$	$\gamma+K$

This transforms the controlled system, after some simple algebraic manipulations, into the form of the uncontrolled system ($K=0$), but with new *effective* values of the parameters $\tilde{\varepsilon}(K)$, $\tilde{\beta}(K)$, and $\tilde{\gamma}(K)$.

For each coupling scheme, the obtained effective parameters and the corresponding transformations are shown in Table I. Since the delayed or shifted quantities are replaced by the fixed point values, the obtained effective parameters $\tilde{\varepsilon}$, $\tilde{\beta}$ and $\tilde{\gamma}$ only depend on K and not on τ or δ.

Although the transformations look rather complex there is a common feature for vv and the two cross-coupling schemes vu and uv: the change in the parameters is such that the fixed point value of the system does not change, i.e., for these three coupling types, the fixed point after the transformation to the system with effective parameters has the same homogeneous fixed point as the system without control. Since for the uu coupling scheme the transformation is more complex, the fixed point in the transformed equations differs from that in the original equations, i.e., the intersection of the nullclines changes its relative position with respect to the cubic nullcline. Note that this does not mean that the fixed point of the original system changes by adding control. Due to the noninvasivity of all investigated control types, the fixed point does not change. However, the transformation that converts the original system with control into a new system without control but effective parameters is, in the case of uu coupling, not invariant for the fixed point (u^*,v^*).

The effects of parameter changes in the FHN system are well known.[3,29] As rule of thumb, one can keep in mind that the larger ε, β, or γ, the lower the excitability of the system.

In the following the K dependence is discussed. In the case of vv coupling, ε does not change. For $K<0$, only β becomes larger, while γ decreases. However, the change in β dominates, i.e., the excitability decreases for $K<0$.

For vu coupling, $\tilde{\varepsilon}$ and $\tilde{\beta}$ increase for $K<0$, while $\tilde{\gamma}$ decreases. In that case the influence of changing $\tilde{\varepsilon}$ dominates, i.e., excitability decreases for $K<0$. For uu and uv coupling, $\tilde{\varepsilon}$ and $\tilde{\beta}$ increase for $K>0$, while $\tilde{\gamma}$ decreases. The influence of $\tilde{\varepsilon}$ dominates, and therefore, the excitability decreases for positive values of K.

For the vv and vu schemes, the inhibitor receives a feedback. In these cases by simply rearranging the inhibitor equation, the original form of the FHN system without control, but with new effective parameters, can be obtained. Therefore no transformation in time and space of the u and v variables has to be performed. For the two coupling schemes, for which the activator receives a feedback (uu and uv), the equations need to be transformed in order to retain the original form without additional control force. In the case of uv, only the v variable is transformed, whereas in the case of uu coupling, both dynamic variables u and v and also time and space are transformed. However, this does not change the qualitative dynamics of the system since transformations in u and v variables and in time and space correspond to rescaling only.

For the two cross-coupling schemes, the effective parameters are symmetric with respect to $K\rightarrow -K$. This symmetry of the cross-coupling schemes was observed in the control domains of all control types (Figs. 4, 6, and 7).

1. Change in excitability

In this section we clarify the influence of the control parameter K on the excitability of the system within the approximation of effective parameters. In particular, the influence of $\tilde{\beta}$ and $\tilde{\gamma}$ is investigated since they change for all control schemes in opposite ways. For vv coupling, the influence of $\tilde{\beta}$ dominates and for the other coupling schemes, the influence of $\tilde{\varepsilon}$ is decisive.

For the three coupling schemes vv, vu, and uv, the transformations from the original system to that with effective parameters leave the fixed point invariant, i.e., the fixed point values with respect to the transformed variables $\tilde{u}$ and $\tilde{v}$ are the same as with respect to the original one (u and v). Since the fixed point depends only on β and γ, the fact that the fixed point remains the same supplies a condition how the effective parameters $\tilde{\beta}$ and $\tilde{\gamma}$ change in dependence of each other. The parameters $-\beta$ and $1/\gamma$ define the intersection with the u axis and the slope of the v-nullcline of the FHN system, respectively. Thus, for a smaller slope of the v-nullcline and unchanged fixed point, $\tilde{\gamma}$ has to be increased and $\tilde{\beta}$ decreased and vice versa. For the three cases of uv, vu, and vv, the dependence between $\tilde{\beta}$ and $\tilde{\gamma}$ yields the condition

$$\tilde{\beta}(\tilde{\gamma}) = \beta + (\gamma - \tilde{\gamma})v^*. \tag{13}$$

It is not intuitively clear how excitability changes. Increasing $\tilde{\gamma}$ while respecting the invariant fixed point condition given by Eq. (13), decreases $\tilde{\beta}$, which yields two opposing effects on excitability. In the following it is shown that under the condition in Eq. (13) the influence of $\tilde{\beta}$ dominates.

To investigate the influence of simultaneously changing $\tilde{\beta}$ and $\tilde{\gamma}$ with unchanged fixed point, numerical simulations of a single FHN systems with effective parameters are performed under the condition in Eq. (13). To excite the system the stimulation current $I(t)$ (inset in Fig. 10) is added to the activator u. The response of the activator u is determined in dependence of $\tilde{\gamma}(K)$. Note that these simulations are done

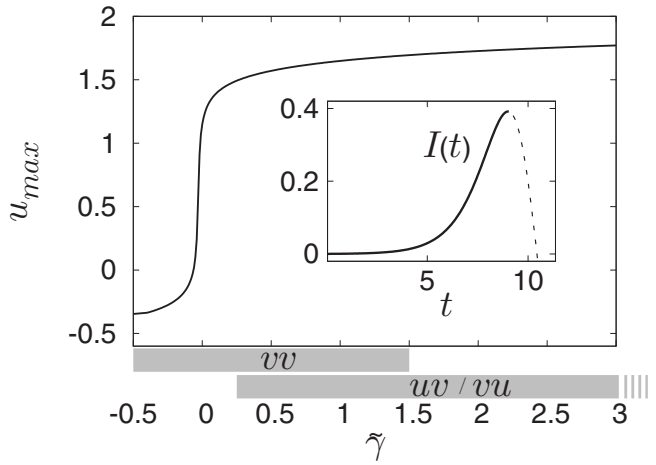

FIG. 10. Maximum amplitude $u_{\max}$ of activator u after stimulation with I(t) (inset: solid line). System parameters: $\varepsilon=0.1$, $\beta=\tilde{\beta}(K)$, and $\gamma=\tilde{\gamma}(K)$. The bars below the x-axis mark the ranges for the effective parameter $\tilde{\gamma}(K)$ for vv coupling and the two cross-coupling schemes uv and vu as K is varied in the range $[-1,1]$.

without feedback. In order to deduce the influence of $\tilde{\beta}$ and $\tilde{\gamma}$ upon excitability, $\tilde{\varepsilon}=\varepsilon=0.1$ is not changed during the simulations. Thus the chosen parameters are equivalent to the effective parameter set of vv coupling. For the other system parameters $\beta=0.85$ and $\gamma=0.5$ are chosen.

In Fig. 10 the maximum amplitude $u_{\max}$ of the activator is plotted versus $\tilde{\gamma}(K)$. For $\tilde{\gamma}(K)<-0.05$, the response of the system to the stimulation $I(t)$ has a small amplitude. For $\tilde{\gamma}(K)>-0.05$, the amplitude of the system blows up in a very tiny parameter range. After this blowup the amplitude remains for all $\tilde{\gamma}(K)>-0.05$ at about the same level.

This blowup resembles the canard explosion of the FHN system near the Hopf bifurcation. The difference is that a canard transition usually characterizes the fast blowup of limit cycles, whereas in the case of an excitable system, a limit cycle does not exist, but only its ghost is visible from the excited trajectories. However, the result is that increasing $\tilde{\gamma}(K)$ with simultaneously adjusting $\tilde{\beta}$ according to Eq. (13) increases the response to a stimulus. We conclude that excitability increases. Therefore it follows that the influence of decreasing $\tilde{\beta}$ dominates. Considering the ranges of $\tilde{\gamma}(K)$ that result for the different coupling schemes by varying K in the interval $[-1,1]$ the impact of each effective parameter on the coupling schemes can be determined.

For the vv coupling scheme, the $\tilde{\gamma}(K)$ is in the interval $[-0.5, 1.5]$ for $K\in[-1,1]$. The excitation of the loop leads to the canardlike blowup close to $\tilde{\gamma}(K)=-0.05$, which is equivalent to $K_{vv}=-0.55$. Hence we estimate for $K_{vv}=-0.55$ a change in excitability. This is in good agreement with the onset of successful control for time-delayed feedback in the spatially extended system [cf. Fig. 7(d)].

For the two cross-coupling schemes uv and vu, the change in $\tilde{\varepsilon}$ dominates. $\tilde{\gamma}(K)$ lies in the interval $[0.25,\infty[$. The values of $\tilde{\gamma}$ for these two schemes are beyond the canardlike transition, in the region of large amplitudes. For the investigated values of K, the system does not undergo the canar-like transition from large to small amplitudes and, hence, the influence of $\tilde{\gamma}$ and $\tilde{\beta}$ on the excitability is small. Therefore the influence of $\tilde{\varepsilon}$ is decisive. To verify this assumption we estimate the value of $K_{uv/vu}$ which is necessary to reach the propagation boundary ∂P by only considering $\tilde{\varepsilon}$. As we know from the numerical computation described in Sec. II B the propagation boundary ∂P for $\beta=0.85$ and $\gamma=0.5$ is reached for $\varepsilon=0.1123$. For larger ε, a stable pulse does not exists. Since the simulations were performed for $\varepsilon=0.1$, one can compute the values of $K_{uv/vu}$ needed to move from $\varepsilon=0.1$ to $\tilde{\varepsilon}=0.1123$, neglecting the influence of $\tilde{\beta}$ and $\tilde{\gamma}$. In the cross-coupling schemes this yields $K_{uv/vu}=\pm 0.123$, which is in very good agreement with the results from the simulations, where successful suppression is found for $|K_{uv/vu}|>0.12$.

Performing the same calculation for the uu coupling assuming that also in that case the influence of ε dominates, $\tilde{\varepsilon}=0.1123$ is reached for $K=0.056$, whereas in the simulations already for $K>0.03$ successful control was observed, which is still of the correct order.

2. Shift of propagation boundary

Above we have introduced effective parameters by replacing the time-delayed or space-shifted quantities in Eqs. (12) and (11), respectively, and have investigated the influence on excitability for one set of system parameters ($\varepsilon=0.1$, $\beta=0.85$, and $\gamma=0.5$) and variable control parameter (K, δ, and τ). In this section the influence of the effective parameters on the propagation boundary ∂P in (ε,β)-parameter space (for $\gamma=0.5$) is compared to the one obtained through simulations with time-delayed feedback. Therefore $|K|=0.2$ and $\tau=0.5\Delta t$ is chosen, where Δt is the temporal pulse width of the activator u. The sign of the control parameter K is chosen such that the excitability is decreased, namely, negative for vv and vu and positive for uu and uv.

The propagation boundaries are obtained in two different ways. Those with time-delayed feedback are obtained by simulating the full equations and performing a bisection method. Those propagation boundaries with effective parameters are obtained by continuation of homoclinic orbits (stationary pulse profiles) in the comoving frame.[3,49]

In Fig. 11 the propagation boundaries ∂P are shown. Those obtained with effective parameters are the full lines separating different colors. The white dashed curves display the propagation boundaries for the full system with time-delayed feedback. The boundaries are in good agreement for vv coupling and the cross-coupling schemes uv and vu. For uu coupling, the two propagation boundary differs from each other. The reason is that the effective parameters are exactly valid for infinitely large τ and are still good approximations for large τ but less so for small τ as shown in the inset of Fig. 11.

The inset shows propagation boundaries of the uu coupling. The full line represents ∂P obtained by effective parameters. The different thin lines represent the propagation boundaries obtained by simulating the full system with different time delays. In the range of small ε for increasing τ, the displayed propagation boundaries of uu coupling converge toward the propagation boundary of the effective pa-

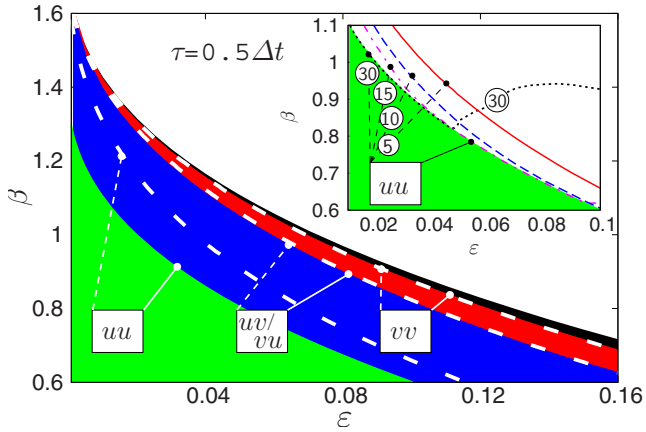

FIG. 11. (Color online) Shift of propagation boundary ∂P: full lines, effective parameters; dashed lines, with time-delayed feedback $\tau=0.5\Delta t$. Inset: propagation boundary for uu coupling: full line, with effective parameters; dashed lines, with different delay times $\tau=5\Delta t$, $\tau=10\Delta t$, $\tau=15\Delta t$, and $\tau=30\Delta t$ (τ is given in units of the pulse width Δt). Parameters: $\gamma=0.5$, $K=0.2$ for uu and uv, $K=-0.2$ for vu and vv.

rameters. The propagation boundary with $\tau=30\Delta t$ perfectly fits the one obtained with effective parameters for $\varepsilon<0.04$. However, for larger ε, this boundary (dotted) diverges sharply from the one with effective parameters. This is caused by the delay-induced bifurcation that occurs for large K and τ (see Sec. IV B 1). Figure 8(c) shows the originating patterns that are already described in Sec. IV B 2. After a local stimulation, the time-delayed feedback suppresses the emerging pulse, as predicted by the effective parameters. However another effect occurs: the feedback is strong enough to create a delay-induced oscillation. This is due to the bistability of the local system, where, in addition to the stable fixed point, a stable and an unstable limit cycle are born in a saddle-node bifurcation. Each of the excitations can spread for a small distance until it is again suppressed by the feedback. Step by step this pattern propagates and grows.

V. DISCUSSION AND CONCLUSION

The increasing interest in both computational investigations of brain functioning[50] and control of complex dynamics[1] has led us to combine methodologies and concepts from both fields to investigate the pathogenesis and potential treatment of brain disorders.[51] This issue sets the context for our studies. However, we expect that our results on controlling traveling pulses can find also applications in other fields of biomedical engineering since traveling pulses occur in many biological systems.[52,53] Furthermore, in this study we consider models and methods of generic type, i.e., on the one side, we study pattern formation in reaction-diffusion (RD) systems of activator-inhibitor type, namely, the FitzHugh–Nagumo (FHN) system, on the other side, stands a universal method of chaos control, that is, time-delayed feedback (Pyragas control[2]), which is used to control the RD patterns. In addition, we consider nonlocal spatial coupling as a control method. Nonlocal spatial coupling and time-delayed feedback have, as we have shown in Sec. IV, a common mechanism that underlies the control of traveling pulses.

The discussion will focus on two issues. First, the comparison of time-delayed feedback and nonlocal spatial coupling, in particular the predictive power of the effective parameters that can be introduced in the same manner in both cases (Sec. V A). Second, the time-delayed feedback and nonlocal spatial coupling will be considered from a broader perspective as augmented transmission capabilities in RD systems with particular respect to the corresponding cortical structures (Sec. V B).

A. Time-delayed feedback and nonlocal spatial coupling

The control force $F(s)$ in Eq. (11), i.e., the force in the anisotropic nonlocal type of coupling with backward connections, can be directly compared to the control force $F(s)$ in Eq. (12), which is time-delayed feedback (Pyragas control) applied to each element in the active media locally. By going from Eq. (12) to Eq. (11), nonlocal connections are introduced simply by changing the position of the shift operator from the first to the second argument of signal $s(x,t)$. In other words, Pyragas control is translated from the temporal to the spatial domain, as illustrated in Fig. 5. This is compatible because the pulse is stationary in the comoving frame and thus the speed of the pulse relates space to time scales. If δ and τ are normalized to the pulse width in the spatial and temporal domain, Δx and Δt, respectively, the common effect of nonlocal coupling and time-delayed feedback on traveling pulses is reflected in similar locations of the control domains in the control planes in Figs. 6 and 7.

The analogy between nonlocal coupling and time-delayed feedback, of course, oversimplifies the situation. However, the use of both types of coupling has been proposed for control of spatiotemporal chaos in spatially extended systems based on the idea of stabilization of unstable periodic patterns embedded in spatiotemporal chaos.[54] Using both types of coupling simultaneously, it has been demonstrated through numerical analysis that unstable roll patterns in a transversely extended three-level laser model can be stabilized. The motivation for this combined approach to control unstable periodic patterns lies in the noninvasive character of both nonlocal coupling and time-delayed feedback if the unstable periodic patterns are approached. Noninvasive refers to the fact that the control force vanishes as the target state is reached.

Our motivation to study nonlocal coupling and time-delayed feedback is somewhat different from that of chaos control because we do not want to stabilize unstable periodic patterns. We investigate the control of traveling pulses by comparing nonlocal coupling with time-delayed feedback using both types separately. We suggest a method to predict the effect of the gain factor K on excitability by identifying the controlled system with the free system with effective parameters based on the idea that the effect of control makes its main contribution upon the front dynamics. Under this assumption, we suggest to replace in both Eqs. (11) and (12) the shifted quantities by their fixed point values, i.e., $s(x,t-\tau)=s(x+\delta,t)=s^*$, where the signal s was chosen to be either u or v, and s^* is the corresponding fixed point value.

Despite its simplicity, this method yields accurate predictions for traveling pulses invading the homogeneous steady state. The resulting equations of effective parameters, given in Table I, describe by simple algebraic relations how control changes excitability (Fig. 2). However, in which direction excitability changes with changing K in the four coupling schemes has to be investigated by evaluating the combined effect on all three effective parameters $\tilde{\varepsilon}$, $\tilde{\beta}$, and $\tilde{\gamma}$ (Fig. 10).

The noteworthy feature of our method is that the effective parameters describe a shift in the excitability of the local elements. By investigating time-delayed feedback in a single local element, it is shown that the onset of pulse suppression as well as the boundedness of the control domains for large K and τ can be explained by the local dynamics. Furthermore, transferring the results of time-delayed feedback to the coupling type of anisotropic nonlocal backward coupling, one finds the same dependences.

B. Reaction-diffusion with augmented transmission as a hybrid model for the cortex

Control introduces augmented transmission capabilities in the RD model (Fig. 3). The resulting hybrid model in Eq. (5) combines the two major signaling systems in the brain, namely local coupling by diffusion, termed volume transmission, and nonlocal coupling in the spatial domain described by Eqs. (10) and (11) or in the temporal domain by Eq. (12). The augmented transmission capabilities are typical for synaptic transmission and neurovascular coupling. For example, the change in sign in the gain parameter K for pulse suppression [Figs. 4(b) and 4(c)] is reminiscent of the Mexican-hat type functional and structural connectivity pattern in the cortex. Also time delays of the order of seconds, that is, the order of the width of the pulse profile Δt in spreading depolarizations (SDs), can occur in synaptic transmission if metabotropic ion channels are involved, such as metabotropic glutamate receptors, which have increased open probabilities in the range of seconds after their activation. Moreover, typical latencies of this order result from the neurovascular coupling. Therefore, the augmented transmission capabilities represent internal neural circuitry that is complementary to the volume transmission introduced in the original Hodgkin–Grafstein equations [Eqs. (1) and (2)] as a model for SDs.

The first hybrid model for SDs that also combines the two major signaling systems in the brain has been studied by Reggia and Montgomery.[55] In this study, potassium dynamics was modeled by a quadratic rate function [cf. Eq. (2)] and coupled to a neural network that mimics cortical dynamics and sensory map organization. At the leading edge of the simulated potassium pulse, the elsewhere largely uniform neural activity was replaced by a pattern of small, irregular patches and lines of highly active elements. The authors explain with this irregular pattern the shape of neurological symptoms in the visual field, as described in migraine patients' reports. However, there is no feedback of the network activity to the potassium RD pulse. Therefore these hybrid models cannot address the questions of the controversially discussed Hodgkin–Grafstein mechanism[56,57] because the augmented transmission capabilities work only one way. In a more general context, such hybrid models are similar to creation of spatiotemporal networks in addressable excitable media, which are studied in the chemical Belousov–Zhabotinskii reaction.[58]

Volume transmission described by the Hodgkin–Grafstein mechanism was long thought to be the main factor that causes the propagation in SDs (Ref. 56) although synaptic transmission and gap junction coupling were suggested to provide an alternative mechanism.[57,59] Hybrid models can address these controversial issue and may help to provide insights into the spread and control of pathological pulses in the brain. Our emphasis is on understanding the role of internal cortical circuits that provide augmented transmission capabilities and can prevent such events. However, a long-term biomedical engineering therapeutic aim is also to design strategies that either support the internal cortical control or mimic its behavior by external control loops and translate these methods into applications.

ACKNOWLEDGMENTS

This work was supported by DFG in the framework of SFB 555. The authors would like to thank Martin Gassel, Erik Glatt, Yuliya Dahlem, Steven Schiff, Ken Showalter, and Hugh Wilson for fruitful discussions.

[1] *Handbook of Chaos Control*, *edited by* E. Schöll and H. G. Schuster (Wiley-VCH, Weinheim, 2008).
[2] K. Pyragas, Phys. Lett. A **170**, 421 (1992).
[3] M. A. Dahlem, F. M. Schneider, and E. Schöll, Chaos **18**, 026110 (2008).
[4] M. Kehrt, P. Hövel, V. Flunkert, M. A. Dahlem, P. Rodin, and E. Schöll, "Stabilization of complex spatio-temporal dynamics near a subcritical Hopf bifurcation by time-delayed feedback," Eur. Phys. J. B (in press).
[5] Y. N. Kyrychko, K. B. Blyuss, S. J. Hogan, and E. Schöll, "Control of spatio-temporal patterns in the Gray-Scott model," Physica D (submitted).
[6] K. A. Richardson, S. J. Schiff, and B. J. Gluckman, Phys. Rev. Lett. **94**, 028103 (2005).
[7] U. B. Barnikol, O. V. Popovych, C. Hauptmann, V. Sturm, H. J. Freund, and P. A. Tass, Philos. Trans. R. Soc. London, Ser. A **366**, 3545 (2008).
[8] M. Lauritzen, Brain **117**, 199 (1994).
[9] N. Hadjikhani and M. Sanchez Del, Proc. Natl. Acad. Sci. U.S.A. **98**, 4687 (2001).
[10] M. Fabricius, S. Fuhr, R. Bhatia, M. Boutelle, P. Hashemi, A. J. Strong, and M. Lauritzen, Brain **129**, 778 (2006).
[11] M. A. Dahlem, F. M. Schneider, and E. Schöll, "Change of spatial excitability by gain controlled time-delayed feedback" (unpublished).
[12] B. Grafstein, in *Brain Function: Cortical Excitability and Steady Potentials*, edited by M. A. B. Brazier (University of California Press, Berkeley, 1963), pp. 87–124.
[13] B. Lindner, J. García-Ojalvo, A. Neiman, and L. Schimansky-Geier, Phys. Rep. **392**, 321 (2004).
[14] G. B. Ermentrout, Rep. Prog. Phys. **61**, 353 (1998).
[15] E. M. Izhikevich, Int. J. Bifurcation Chaos Appl. Sci. Eng. **10**, 1171 (2000).
[16] A. T. Winfree, Chaos **1**, 303 (1991).
[17] Y. A. Kuznetsov, *Elements of Applied Bifurcation Theory* (Springer, New York, 1995).
[18] M. A. Dahlem and S. C. Müller, Exp. Brain Res. **115**, 319 (1997).
[19] A. T. Winfree, Science **266**, 1003 (1994).
[20] A. S. Mikhailov and V. S. Zykov, Physica D **52**, 379 (1991).
[21] Z. Nagy-Ungvarai, J. Ungvarai, and S. C. Müller, Chaos **3**, 15 (1993).
[22] M. Braune and H. Engel, Chem. Phys. Lett. **204**, 257 (1993).
[23] J. Schlesner, V. Zykov, H. Engel, and E. Schöll, Phys. Rev. E **74**, 046215 (2006).
[24] M. A. Dahlem and S. C. Müller, Ann. Phys. **13**, 442 (2004).
[25] M. A. Dahlem and N. Hadjikhani, "Migraine aura: retracting particle-like waves in weakly susceptible cortex," PLoS ONE (in press).

[26]T. Sakurai, E. Mihaliuk, F. Chirila, and K. Showalter, Science **296**, 2009 (2002).
[27]V. S. Zykov and K. Showalter, Phys. Rev. Lett. **94**, 068302 (2005).
[28]A. S. Mikhailov and K. Showalter, Phys. Rep. **425**, 79 (2006).
[29]M. A. Dahlem, F. M. Schneider, and E. Schöll, J. Theor. Biol. **251**, 202 (2008).
[30]F. Schlögl, Z. Phys. **253**, 147 (1972).
[31]H. R. Wilson, *Spikes, Decisions, and Actions: The Dynamical Foundations of Neuroscience* (Oxford University Press, Oxford, 1999).
[32]E. Schöll, *Nonlinear Spatio-Temporal Dynamics and Chaos in Semiconductors* (Cambridge University Press, Cambridge, 2001).
[33]J. L. Hindmarsh and R. M. Rose, Nature (London) **296**, 162 (1982).
[34]K. F. Bonhoeffer, Naturwiss. **40**, 301 (1953).
[35]R. FitzHugh, Biophys. J. **1**, 445 (1961).
[36]J. Nagumo, S. Arimoto, and S. Yoshizawa, Proc. IRE **50**, 2061 (1962).
[37]H. Kager, W. J. Wadman, and G. G. Somjen, J. Neurophysiol. **84**, 495 (2000).
[38]G. Florence, M. A. Dahlem, A. C. G. Almeida, J. W. M. Bassani, and J. Kurths, "The role of extracellular potassium dynamics in the different stages of ictal bursting and spreading depression: A computational study," J. Theor. Biol. (in press).
[39]M. Gassel, E. Glatt, and F. Kaiser, Fluct. Noise Lett. **7**, L225 (2007).
[40]M. Gassel, E. Glatt, and F. Kaiser, Phys. Rev. E **77**, 066220 (2008).
[41]This corrects Eq. (7) in Ref. 3.
[42]A. Hutt, Phys. Rev. E **70**, 052902 (2004).
[43]B. Fiedler, V. Flunkert, M. Georgi, P. Hövel, and E. Schöll, Phys. Rev. Lett. **98**, 114101 (2007).
[44]T. Dahms, P. Hövel, and E. Schöll, Phys. Rev. E **76**, 056201 (2007).
[45]P. C. Bressloff, Physica D **155**, 83 (2001).
[46]M. A. Dahlem, G. Hiller, A. Panchuk, and E. Schöll, "Dynamics of delay-coupled excitable neural systems," Int. J. Bifurcation Chaos Appl. Sci. Eng. (to be published), e-print arXiv:0803.2352.
[47]E. Schöll, G. Hiller, P. Hövel, and M. A. Dahlem, Philos. Trans. R. Soc. London, Ser. A **367**, 1079 (2009).
[48]N. Manz, B. T. Ginn, and O. Steinbock, Phys. Rev. E **73**, 066218 (2006).
[49]B. Sandstede, in *Handbook of Dynamical Systems*, edited by B. Fiedler (Elsevier/North-Holland, Amsterdam, 2002).
[50]See this Focus Issue.
[51]E. Ruppin, J. A. Reggia, and D. Glanzman, Prog. Brain Res. **121**, ix (1999).
[52]J. M. Davidenko, P. F. Kent, D. R. Chialvo, D. C. Michaels, and J. Jalife, Proc. Natl. Acad. Sci. U.S.A. **87**, 8785 (1990).
[53]P. Camacho and J. D. Lechleiter, Science **260**, 226 (1993).
[54]W. Lu, D. Yu, and R. G. Harrison, Phys. Rev. Lett. **76**, 3316 (1996).
[55]J. A. Reggia and D. Montgomery, Comput. Biol. Med. **26**, 133 (1996).
[56]A. J. Strong, J. Neurophysiol. **94**, 5 (2005).
[57]O. Herreras, J. Neurophysiol. **94**, 3656 (2005).
[58]M. Tinsley, J. Cui, F. V. Chirila, A. Taylor, S. Zhong, and K. Showalter, Phys. Rev. Lett. **95**, 038306 (2005).
[59]B. E. Shapiro, J. Comput. Neurosci. **10**, 99 (2001).